



# European Commission's 7<sup>th</sup> Framework Programme Grant Agreement No. **226520**

Project acronym: COMBINE

# Project full title: Comprehensive Modelling of the Earth System for Better Climate Prediction and Projection

Instrument: Collaborative Project & Large-scale Integrating Project

Theme 6: *Environment* Area 6.1.1.4: *Future Climate* 

ENV.2008.1.1.4.1: New components in Earth System modelling for better climate projections

Start date of project: 1 May 2009 Duration: 48 Months

# Deliverable Reference Number and Title: D3.3 Troposphere-stratosphere system in the tropics

Lead work package for this deliverable: WP3

Organization name of lead contractor for this deliverable: MPG

Due date of deliverable: 36 Actual submission date: 54

Project co-funded by the European Commission within the Seven Framework Programme (2007-2013)		
Dissemination Level		
PU	Public	X
PP	Restricted to other programme participants (including the Commission Services)	
RE	Restricted to a group specified by the consortium (including the Commission Services)	
CO	Confidential, only for members of the Consortium (including the Commission Services)	

# **D3.3** Troposphere-stratosphere system in the tropics

The goal of COMBINE WP3 was to include the stratosphere in participating Earth System Models and carry out a selected subset of CMIP5 simulations with the newly developed models. This report concerns the analysis of CMIP5 *pre-industrial control* and/or *historical* simulations done with the newly developed models, with focus on the troposphere-stratosphere system in the tropics. Three topics are addressed: (1) Tropical oscillations; (2) Equatorial waves; and (3) Water vapor distribution. Particular emphasis on the evaluation of QBO related aspects is placed in the work carried out for topic (1) and (2), while topic (3) covers annual mean, seasonal cycle & inter-annual variability and trends.

# 1. Tropical Oscillations

#### 1.1 Introduction

The equatorial stratospheric wind exhibits distinct oscillations known as the quasibiennial oscillation (QBO), extending vertically from about 100 to 5 hPa, and the semiannual oscillation (SAO) at the stratopause. The QBO depends on the deposition of zonal momentum carried upward by vertically propagating waves, which dissipate in the regions of wind shear. The westerly phase of the SAO as well is the result of momentum deposition, while its easterly phase is mainly due to equatorwards advection of summer hemispheric easterlies. The sources of the vertically propagating waves, driving the QBO and SAO, are mostly in the troposphere. While the QBO is driven by waves dissipating or breaking in the stratosphere, hence still relatively close to their sources, the SAO is forced by waves that have survieved filtering by QBO winds. Thus, the Equatorial atmosphere is vertically coupled through the existence of a vertically propagating wave spectrum, with originates in the troposphere and is filtered by wave mean- flow interaction higher up.

The simulation of the QBO and the SAO has been a persistent challenge in climate modelling for two main reasons: (1) lack of vertical extent and resolution, and (2) insufficient excitation of waves, in part related to a lack of both horizontal and vertical resolution, limiting generation mechanisms.

The COMBINE project now includes climate models – CMCC-CMS, HadGEM2-CC and MPI-ESM-MR – which extend vertically to the mesosphere and have a high enough vertical resolution to allow for the simulation of the QBO, while incorporating gravity wave parameterization to account for the lack of a sufficiently high horizontal resolution. The purpose of the following analysis is to assess the quality of the simulated QBO and SAO, by comparisons between re-analyses and model simulations. The comparison includes the three model systems mentioned above and in addition the Japanese MIROC Earth system model, which also simulates a QBO.

The comparison makes use of ECMWF reanalyses: ERA-40 (from 1970 to 1999, Uppala et al. 2005) and ERA-interim (from 1979to 2010, Dee et al. 2011); and *pre-industrial control* simulations (*piControl*) following the specifications of CMIP5 (Taylor et al. 2012), for: CMCC-CMS (Manzini et al 2012), HadGEM2-CC (Martin et

al. 2013) MPI-ESM-MR (Giorgetta et al. 2013) and MIROC-ESM (Watanabe et al. 2011). For a detailed analysis of the QBO in MPI-ESM-MR see Krismer et al. (2013).

# 1.2 Time series of monthly and zonally averaged zonal wind at the Equator

A view of the absolute amplitudes, vertical extent, period and regularity of the QBO and the SAO in monthly and zonally averaged zonal winds is shown in Figure 1.1, for a subset of arbitrary selected 14-year periods. The QBO main features agree well in ERA-40 and ERA-interim, during the years when the two datasets overlap. As the QBO is an internal mode of variability, the QBO time series in the model simulations can be in arbitrary phase relationship between each other and the observations. It is not to expect that the observed time series is reproduced, and a comparison of model results and re-analyses data aims to assess typical features of the QBO, like the frequency, the amplitude and the vertical structure, examined hereafter.

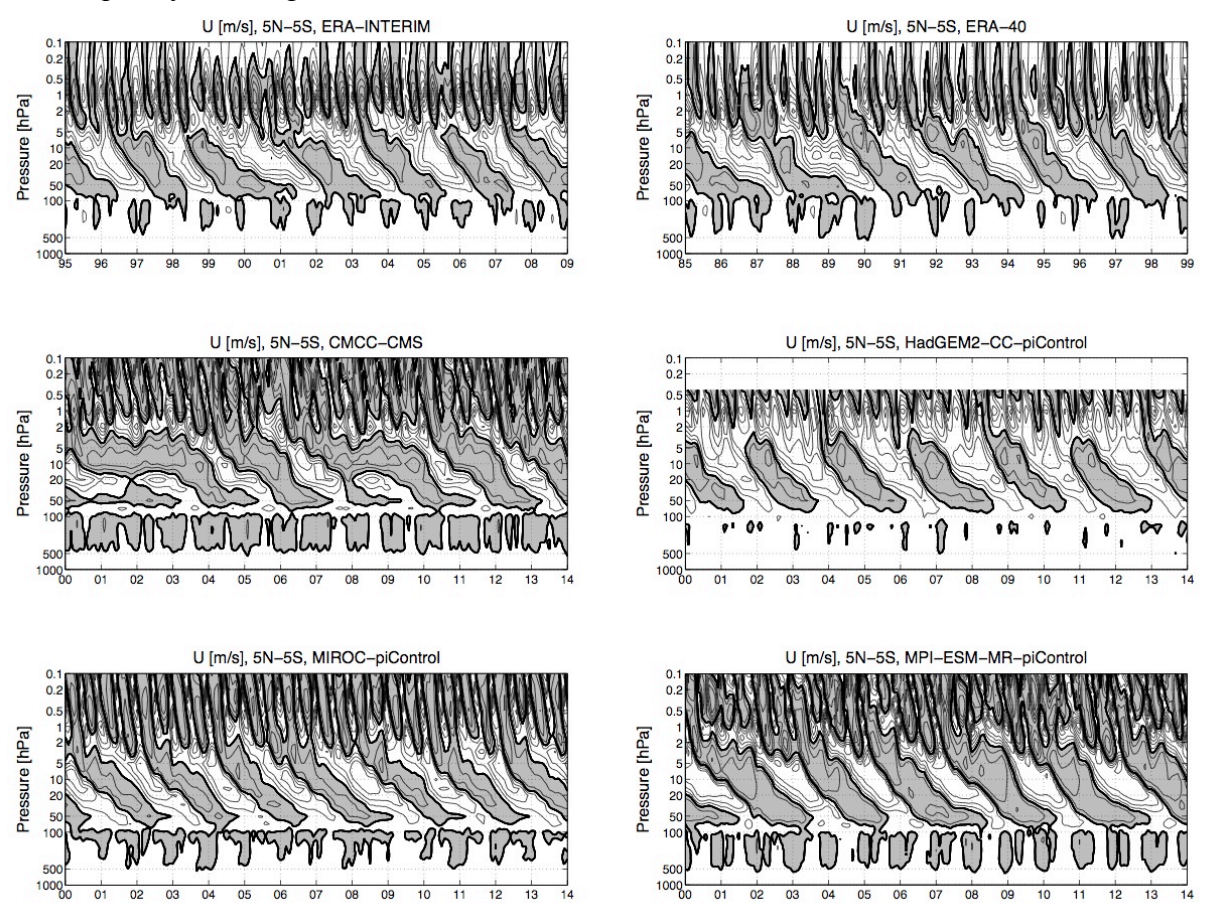


Figure 1.1: Time-height section at the Equator of the monthly and zonally averaged zonal wind: ERA-Interim, 1995-2008, and ERA-40, 1985-1998 (top), CMCC-CMS and HadGEM2\_CC (middle), MIROC and MPI-ESM-MR (bottom). The contour interval is 10 m/s. Positive wind speeds are shaded in grey. The thick contour line indicates the zero wind line.

All models clearly show low frequency oscillations of the zonally averaged zonal wind in the Equatorial stratosphere. Deviations from the observations are found for various properties of the QBO. The most obvious one consist in the occasional prolongation of westerly winds above 20 hPa in CMCC-CMS, as occurring twice in the selected period. Still, the westerly winds between 20 and 70 hPa alternate with a

period close to two years. This behavior has not been observed. However, such episodes in CMCC-CMS show that equatorial westerly jets may exist near 50 hPa without a direct link to a westerly jet descending form higher altitudes. Between 50 and 70 hPa, the occasional stalling of the easterly phase appears more evidently in CMCC-CMS and MPI-ESM-MR than in HadGEM2-CC and MIROC-ESM. In the troposphere, CMCC-CMS and MPI-ESM-MR tend to have a westerly bias and HadGEM2-CC an easterly bias.

# 1.3 Equatorial variability

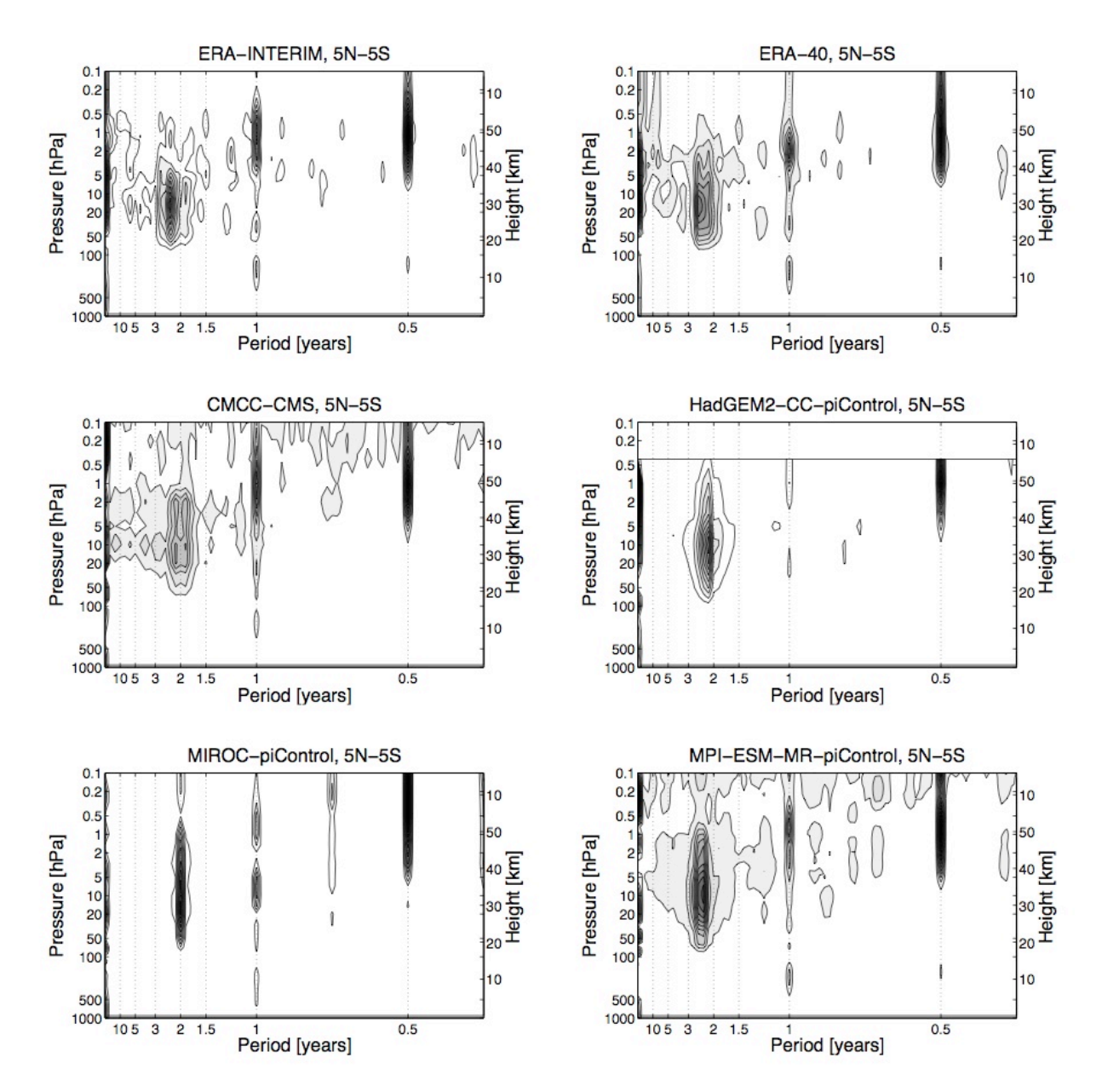
The variability of the Equatorial atmosphere is depicted in Figure 1.2, showing the zonal wind amplitude as a function of Fourier-harmonics computed as in Pascoe et al. (2005, their Figure 3). To compute the amplitude, the 600-year *piControl* runs have been split into 30-year time windows with 3-year overlap (approximately one quasibiennial cycle) between each window. Then, a fast Fourier-transform in time has been applied to the zonally and meridionally (5°N-5°S) averaged data in each window, which thus, have 360 Fourier harmonics. The amplitude is the absolute value of the Fourier-coefficients. The amplitudes have been averaged at every harmonic over all time windows. For the Singapore and ERA data, which do not cover more than 50 years, the last 30 years of the datasets have been chosen to perform the Fourier-transform.

Figure 1.2 shows that an annual cycle (period one year) in zonal winds is clearly present in the troposphere, stratosphere, and lower mesosphere, for all datasets but HadGEM2-CC. This latter model exhibits a rather weak annual cycle. The MIROC model underestimates the 0.5-5 hPa peak of the annual model, seen in both re-analysis datasets, as well as in CMCC-CMS and MPI-ESM-MR. Above 5 hPa at the period of 6 months, the two ERA-reanalysis and all the models show a strong peak in amplitude associated with the semi-annual oscillation.

For periods longer than 1.5 years, all datasets show large amplitudes between 1 and 100 hPa, the manifestation of the QBO. ERA-40 and ERA-interim amplitudes peak between two and three years, and between 10-20 hPa. The spectral signature of the QBO differs somewhat across the models. CMCC-CMS shows a weaker and broader peak extending at higher altitudes, which illustrates the irregularity of the QBO shown in Figure 1.1. The widths of the QBO spectral peaks in HadGEM2-CC and MPI-ESM compare well with ERA-40, however it is too narrow in MIROC. The narrow distribution of the amplitude in MIROC around 24 months indicates some phase locking with the annual cycle.

The variability in the QBO period is illustrated by histograms (Figure 1.3). To construct Figure 1.3, the QBO period is measured as the time between two subsequent onsets of QBO westerly jets at 20 hPa. Here we have also included information from radiosonde observations at Singapore, 1953-2011 (Naujokat et al., 1986; http://www.geo.fu-berlin.de/en/met/ag/strat/produkte/qbo/). The model histograms are based on arbitrary selected 100-year periods of the respective *piControl* experiment. Hence the model histograms include significantly more QBO cycles than the Singapore record or the ECMWF re-analyses.

In Singapore as well as in the re-analyses, the QBO period differs from cycle to cycle by more than one year. Singapore shows periods between 19 and 34 months, with an average of 27 months. In ERA-40, the minimum, average and maximum period are 24 27 and 33 months, respectively. ERA-interim tends to have a distribution spread towards longer periods. The QBO period in ERA-interim has a slightly larger range due to the QBO cycles that occurred after the end of ERA-40 at 1999.



*Figure 1.2:* Amplitude of Fourier harmonics as a function of altitude and corresponding period for ERA- interim and ERA-40 (top), CMCC-CMS and HadGEM2-C (middle) and MIROC and MPI-ESM-MR (bottom). The contour interval is 3 m/s.

The minimum, average and maximum QBO periods are 22, 25, and 31 months in HadGEM2-CC and 24, 29, and 34 months in MPI-ESM-MR, in good agreement with the ERA-40 and Singapore estimates. The distribution of the QBO period in MIROC shows a high peak at 24 months and relatively little variability, which again indicates a dynamical phase locking between the QBO and the annual cycle. In CMCC-CMS,

the average QBO period amounts to 24 months, however, the spread of the periods is significantly larger than at Singapore or for the reanalysis. The tail of short cycles in the histogram is due to the fact that occasionally the zero wind line oscillates forth and back across the 20 hPa level, with each of this transitions measured separately by the employed algorithm.

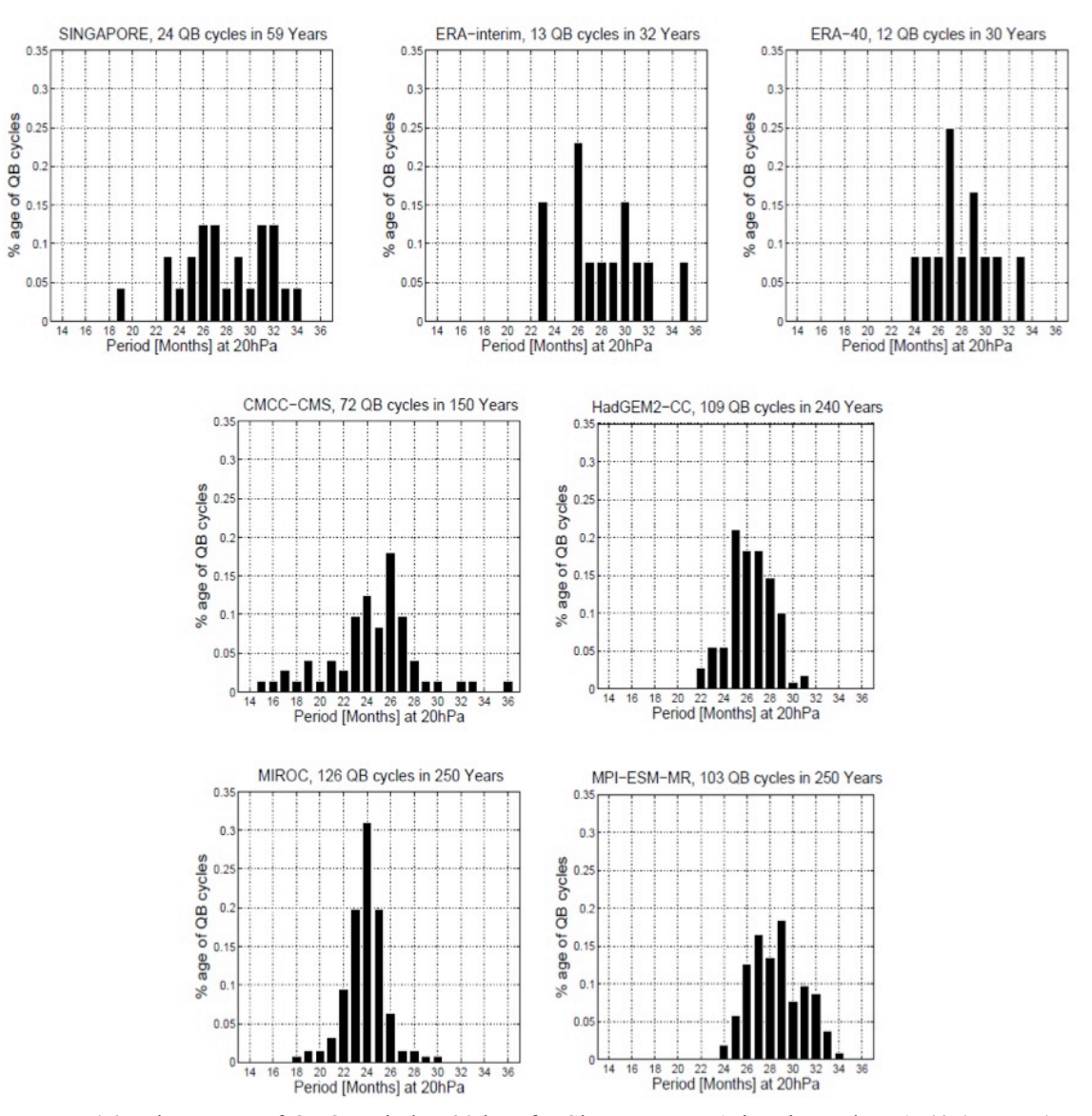


*Figure 1.3:* Histograms of QBO period at 20 hPa for Singapore, ERA-interim and ERA-40 (top row), CMCC-CMS and HadGEM2-C (middle row) and MIROC and MPI-ESM-MR (last row).

# 1.4 Amplitude Profiles

Figure 1.4 shows the peak-to-peak amplitudes of the QBO (solid) and the SAO (dashed). The peak-to-peak amplitudes have been calculated following Baldwin and Gray (2005), as  $2\sqrt{2}\sigma$ , where  $\sigma$  is the standard deviation of the zonal wind due to the QBO and the SAO. Band pass filters of 20 to 40 months and 6 months have been used to isolate the QBO and the SAO signal, respectively. Magnitude and vertical extend of the peak-to-peak QBO amplitudes in CMCC-CMS, HadGEM2-CC and MIROC are in general good agreement with ERA-40, while MPI-ESM-MR substantially

overestimates this amplitude above 20 hPa. In general, all models tend to overestimate, to a different degree, the QBO amplitude above 10 hPa. Consequently, CMCC-CMS, HadGEM2-CC and MPI-ESM-MR show the largest QBO amplitude around 10 hPa, whereas in ERA-40, the QBO is strongest at 20 hPa.

Concerning the SAO amplitude, the models generally show peak-to-peak amplitudes, which are larger (to a different degree) than in ERA-40 (dashed lines in Figure 1.4) and that maximize at lower pressure levels. With respect to ERA-Interim, the modeled SAO amplitudes are instead slightly underestimated. A caveat in the comparison with the SAO peak-peak amplitude estimated by ERA-40 is that vertical resolution is low at these elevations in ERA-40. The model used for ERA-Interim has more vertical levels in the upper stratosphere and can possibly better resolve the uppermost stratosphere.

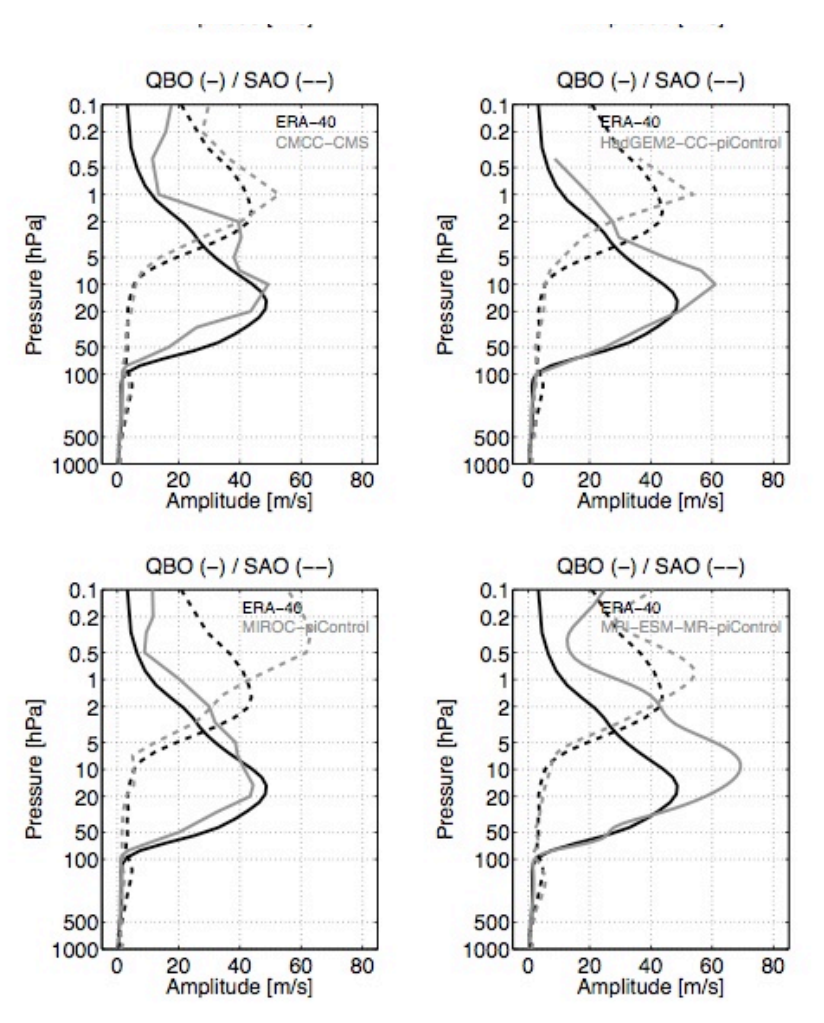


Figure 1.4: Amplitude in zonal wind in m/s due to the QBO (solid lines) and the SAO (dashed lines) for ERA-40 (black line) and models: CMCC-CMS and HadGEM2-CC (top) and MIROC and MPI-ESM-MR (bottom). Band pass filters of 20 to 40 months and 6 months have been used to isolate the QBO and the SAO signal, respectively.

#### 1.5 Composites of the QBO in zonal wind

Figure 1.5 shows composites of the time height sections of the quasi-biennial cycle in the monthly and zonally averaged Equatorial zonal wind in the ERA-40 reanalysis and in the models. The composite (averaged) cycle is constructed by first finding the

onset of the QBO westerly jet at 5 hPa (the central month, relative time = 0) and then computing averages of the zonal wind over all months with the same distance in time to the central month. To keep the information about the semi-annual oscillation, only QBO phase changes occurring at 5 hPa in May have been chosen for the composites (see also Krismer et al., 2013). Thus, Figure 1.5 can depict a connection between the westerly jets of the SAO and QBO.

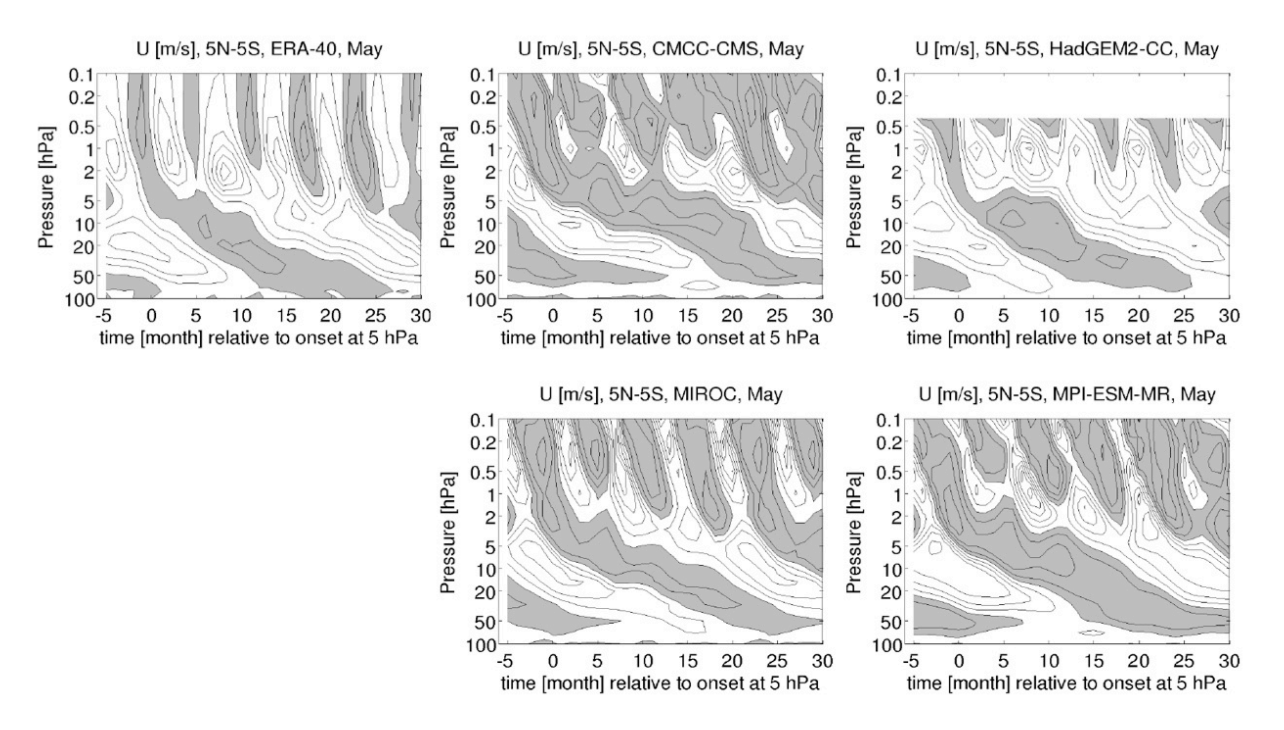


Figure 1.5: Time-height section of the composite (see text) of Equatorial zonal mean zonal wind in ERA-40, CMCC-CMS and HadGEM2\_CC (top panel) and in MIROC and MPI-ESM-MR (lower panel). The contour interval is 10 m/s. Positive wind speeds are shaded in grey. The thick contour line indicates the zero wind line.

Such an initialization of the QBO jets by the SAO has been proposed by the very first theory on the QBO by Lindzen and Holton (1968) but set aside later as not strictly necessary for the existence of the QBO (Holton and Lindzen 1972). Evidence for the SAO influence on the QBO in radiosonde observations, ERA-40 and models is given by Dunkerton and Delisi (1997), Kuai (2009) and Krismer (2013). Figure 1.5 shows that in the models assessed, the SAO westerly jet can further propagate downward, while its phase progression rate decreases, giving origin to the OBO.

To further investigate the connection between SAO and QBO, Figure 1.6 shows the distribution of the onset of the QBO westerly jet at 5 hPa throughout the year. The distributions in ERA-40 and in all models cluster around May and October. Computing composites based on the onset of the westerly jets at 5 hPa from April to June or from September to November, when according to Figure 1.6 more than 90 % of the westerly jets are initiated, would show the same connection between the SAO westerly jet as shown in our current Figure 1.5. From this we conclude that in the models (especially in MIROC) the onset of the QBO westerly jet is strongly linked to the occurrence of the SAO westerly jet.

Figure 1.5 also shows the main features of the QBO in the respective models. Above 20 hPa, the QBO westerly jets in CMCC-CMS and MPI-ESM-MR are too strong compared to the re-analysis. The QBO easterly jets in these models are as strong as in ERA-40. HadGEM2-CC and MIROC have about the same amplitude of the QBO westerly and easterly jets as ERA-40.

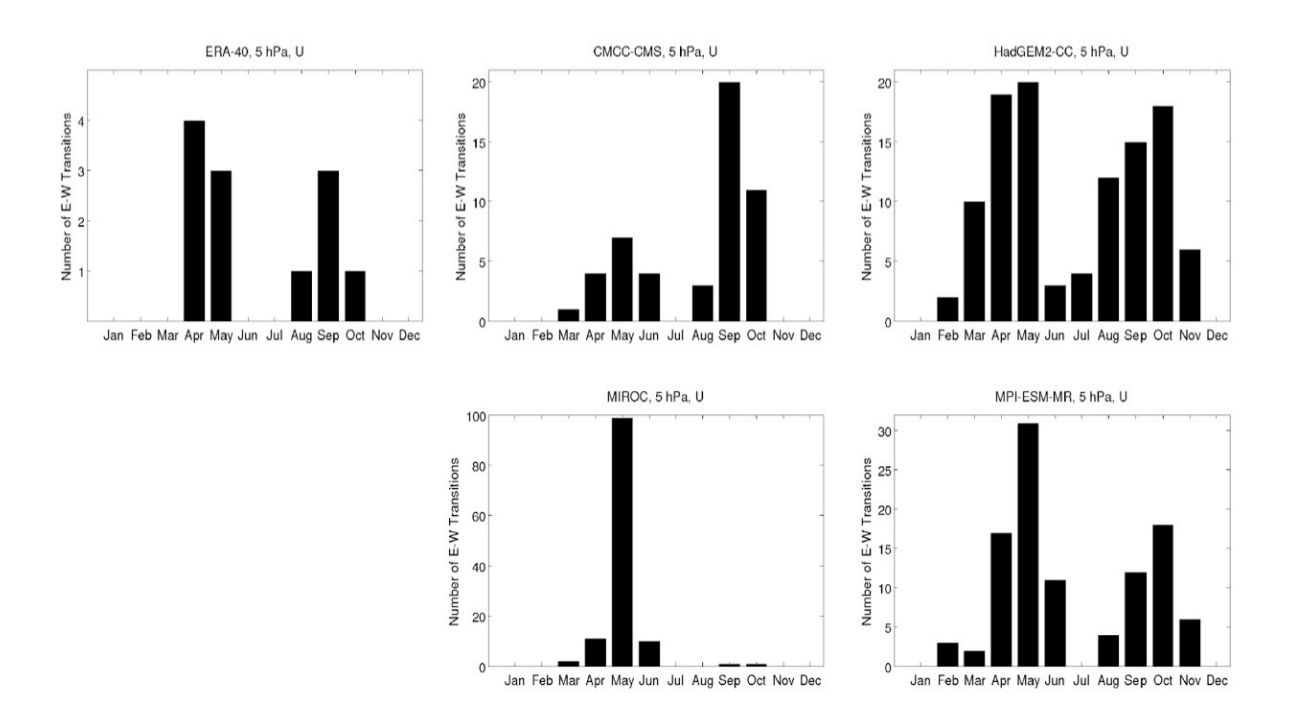


Figure 1.6: Monthly distribution of the onset of the QBO westerly jet at 5 hPa in ERA-40, CMCC-CMS and HadGEM2\_CC (top panel); in MIROC and MPI-ESM-MR (lower panel).

#### 1.6 Average annual cycle

In both ERA re-analysis, the SAO jets, which are strongest at 1 hPa, propagate down to 5 hPa (Figure 1.7). The amplitude of the SAO is stronger during the semiannual cycle starting in December and ending in June (repeated twice in Figure 1.7), when the easterly and westerly jets reach -40 m/s and +30 m/s (in ERA-Iterim), respectively. In July and October, the jets are weaker than -10 and +15 m/s, respectively. The main difference between ERA-40 and Interim is a stronger westerly jet in ERA-Interim in April. The annual modulation of the SAO amplitude is associated with a stronger meridional momentum advection in boreal winter (Delisi and Dunkerton 1988).

The modelled SAO differs somewhat between the models. In HadGEM2-CC, the SAO westerly jets are not well resolved. In the other models, there seems to be a tendency to a westerly bias, from the troposphere to the mesosphere, Particularly in CMCC-CMS. In addition, the cores of the SAO westerly jets are located higher than in the reanalysis. Further, MIROC and MPI-ESM-MR underestimate the annual cycle of the SAO westerly jets amplitude. The cores of the SAO easterly jets are located at the approximately right altitude in CMCC-CMS, HadGEM2-CC and MPI-ESM-MR, but too high in MIROC. The amplitudes of the SAO easterly jet and its annual modulation are well represented in all models.

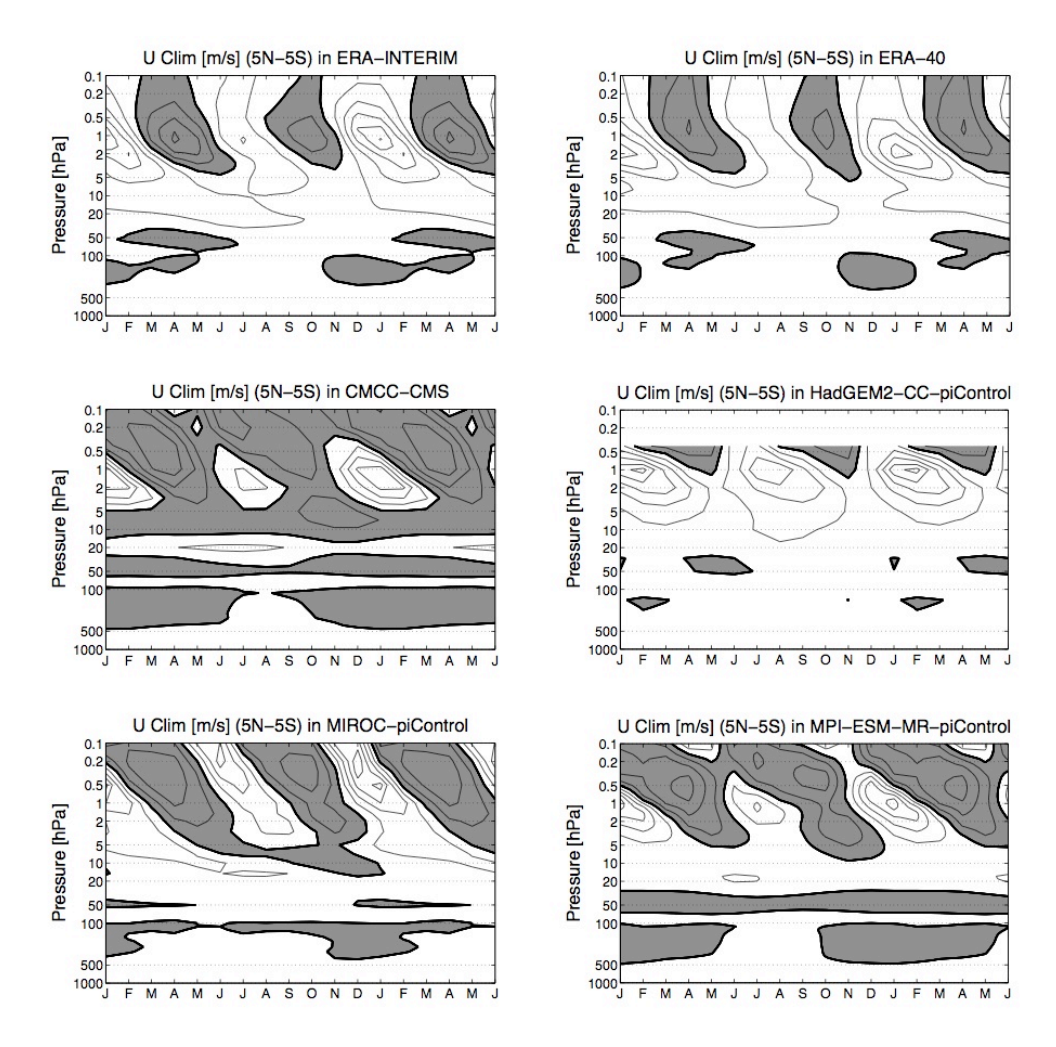


Figure 1.7: Climatological annual cycle of monthly and zonally averaged zonal wind (m/s) at the Equator: ERA-Interim and ERA-40 (top), CMCC-CMS and HadGEM2\_CC (middle), MIROC and MPI-ESM-MR (bottom). The contour interval is 10 m/s. Positive wind speeds are shaded in grey. The thick contour line indicates the zero wind line.

#### 1.7 Summary

The main features of the QBO and the SAO in the general circulation models CMCC-CMS, HadGEM2-CC, MIROC and MPI-ESM-MR have been compared to radiosonde observations from Singapore and ECMWF re-analysis products, ERA-40 and ERA-interim. In the Equatorial stratosphere, HadGEM2-CC, MIROC and MPI-ESM-MR show a quasi-regular oscillation of easterly and westerly jets. The CMCC-CMS model shows instead frequent stalling of the QBO westerly jet in the upper stratosphere, a feature not observed. The distribution of the QBO periods is too narrow in HadGEM2-CC and MIROC models, compared to the observations and the re-analysis, which indicates a too regular QBO. MPI-ESM-MR has a more realistic distribution of the QBO period; however, largely overestimate the QBO amplitude above 20 hPa. For all models, QBO amplitudes compare well with reanalysis up to 20 hPa. All models show a link between the westerly jets of the SAO and the westerly jets of the QBO, which indicates the seeding of the QBO westerly jets by the SAO.

The modeled amplitude of the SAO is within the ERA-40 and ERA-Interim range. However, MIROC and MPI-ESM-MR, overestimate the strength of the SAO westerly jet in fall, while HadGEM2-CC underestimates the downward propagation of the SAO westerly jets. CMCC-CMS, MIROC and MPI-ESM-MR capture to a large degree the annual modulation of the SAO. Overall, however, this new set of coupled climate models succeeds in simulating the QBO, unlike their predecessor models used for CMIP3.

## References

- Baldwin, M. P., L. Gray (2005) Tropical stratospheric zonal winds in ECMWF ERA-40 reanalysis, rocketsonde data, and rawinsonde data. Geophys. Res. Lett., 32(9):2–6.
- Dee et al. (2011) The ERA-Interim re-analyses: configuration and performance of the data assimilation system. Q. J. R. Meteorol. Soc., 137, 553–597, DOI: 10.1002/qj.828.
- Delisi, D. P., T. J. Dunkerton (1988) Seasonal variation of the semiannual oscillation. J. Atmos. Sci., 45(19), 2772–2787
- Dunkerton, T. J., D. P. Delisi (1997) Interaction of the quasi-biennial oscillation and stratopause semiannual oscillation. J. Geophys. Res., 102(D22), 26107–26116.
- Giorgetta, M. A. et al. (2013) Climate and carbon cycle changes from 1850 to 2100 in MPI-ESM simulations for the Coupled Model Intercomparison Project phase 5. J. Adv. Model. Earth Syst., 5, doi:10.1002/jame.20038.
- Holton, J., R. Lindzen (1972) An updated theory for the quasi-biennial cycle of the tropical stratosphere. J. Atmos. Sci., 29(6), 1076–1080
- Krismer, T. R., M. A. Giorgetta, M. Esch (2013) Seasonal Aspects of the Quasi-Biennial Oscillation in MPI-ESM and ERA-40. J. Adv. Model. Earth Syst., 5, 406–421, doi:10.1002/jame.20024.
- Kuai, L., et al. (2009) Nonstationary synchronization of equatorial QBO with SAO in observations and a model. J. Atmos. Sci., 66(6), 1654–1664.
- Lindzen, R., J. Holton (1968) A Theory of the quasi-biennial oscillation. J. Atmos. Sci., 25, 1095–1107.
- Martin, G. M. et al. (2011) The HadGEM2 family of Met Office Unified Model Climate configurations. Geosci. Model Dev., 4, 765-841, doi:10.5194/gmd-4-723-2011.
- Manzini, E., et al. (2012) Stratosphere Troposphere coupling at interdecadal time scales: Implications for the North Atlantic Ocean. Geophys. Res. Lett. 39, L05801, doi:10.1029/2011GL050771.
- Naujokat, B. (1986) An update of the observed quasi-biennial oscillation of the stratospheric winds over the tropics. J. Atmos. Sci. 43, 1873–1877.
- Pascoe, C. L. et al. (2005) The quasi-biennial oscillation: Analysis using ERA-40 data. J. Geophys. Res., 110(D8):1–13.
- Taylor, K. E., R. J. Stouffer, G. A. Meehl (2012) An Overview of CMIP5 and the Experiment Design. Bull. Amer. Meteor. Soc., 93, 485–498, doi:10.1175/BAMS-D-11-00094.1.
- Uppala et al. (2005) The ERA-40 re-analysis. Q. J. R. Meteorol. Soc., 131, 2961-3012.
- Watanabe, S., et al. (2011) MIROC-ESM 2010: model description and basic results of CMIP5-20c3m experiments. Geosci. Model Dev., 4, 845-872, doi:10.5194/gmd-4-845-2011, 2011.

# 2. Equatorial waves

The Equatorial wave analysis has lead to a manuscript "Kelvin and Rossby gravity wave packets in the lower stratosphere of some high-top CMIP5 models", by Lott, F. et al., submitted to Journal of Geophysical Research (under review). Here the abstract is reported:

**Abstract**. This study shows that the CMIP5 models considered can simulate realistic aspects of Kelvin and Rossby-gravity wave packets with periods of a few days and that freely propagate into the lower stratosphere. The models seem to represent better these stratospheric waves than the tropospheric convectively coupled waves analyzed in previous papers. There is nevertheless a large spread among models. Those with a

Quasi-Biennial Oscillation (QBO) in the Equatoral stratosphere tend to produce larger waves than (i) the models without QBO and (ii) the ERA-Interim reanalysis. For the Rossby-gravity waves this is simply explained by the fact that models without a QBO do not have westerly winds in the lower stratosphere, a situation that is favorable to the propagation of Rossby-gravity waves. For the Kelvin waves, the explanation is not as straightforward, since in models with a QBO, the Kelvin waves are larger when the zonal mean zonal wind is negative, a situation always satisfied in models without a QBO. We attribute the difference to the fact that models with a QBO also have finer vertical resolution in the stratosphere. We also analyze the influence of precipitation and find a tendency for the models with large precipitation variability to have larger waves. The effect is nevertheless not as pronounced as was found in previous papers. In fact, even models with weak precipitation variability still have quite realistic waves in the lower stratosphere, indicating either that (i) other sources can be significant or that (ii) the dynamical filtering strongly mitigates the differences in wave sources between models.

# 3. Water vapour distribution

#### 3.1 Introduction

Variations of the global water vapor into the lower stratosphere are not only impacting radiative balance of the Upper Troposphere Lower Stratosphere (UTLS) region, but can act as an important driver of decadal global surface climate change. Solomon et al. (2010) have shown that about 10% decrease of stratospheric water vapor in the lower stratosphere between 2001-2005 has counteracted about 25% of global surface temperature increase due to well mixed greenhouse gases, specifically they estimate that a reduction of water vapor in the 2001-2005 period with respect to 1996-2000 resulted in a radiative forcing of about -0.1 Wm<sup>-2</sup> partially offsetting the +0.26 Wm<sup>-2</sup> due to increase of CO<sub>2</sub>. Moreover, changes of stratospheric H<sub>2</sub>O can have impact on stratospheric O<sub>3</sub> and its recovery. The UTLS budget of water vapor is determined by several processes: Tropospheric convection leading to localized moistening, dehydration, horizontal advection trough cold trap regions, precipitating cirrus, and convective mixing (Randel and Jenkins 2013, for a review). At interannual time scales, the Quasi Biennial Oscillation (QBO) and the El Nino Southern Oscillation (ENSO) determine water vapor variability in the tropical regions. Water vapor concentration in the UTLS region has been reconstructed by tracing a parcel history back to the coldest temperature it experiences (the Lagrangian Cold Point, LCP) with ENSO and QBO impacting LCP: 1 K change in the cold point temperature can lead to 0.5 ppm change in water vapor (Fueglistaler and Haynes 2005).

The analysis reported here focuses on the evaluation of the representation of water vapor in the high-top (HT) and low-top (LT) models participating in the CMIP5 exercise. The modeled water vapor is compared to HALOE observations. The CMIP5 historical simulations are used in the comparison. This analysis is subdivided in the following parts: Annual mean climatology; Seasonal cycle; Inter-annual variations associated to ENSO and the Asian Monsoon; and Trends. At inter-annual timescales, QBO and volcanic eruptions impact water vapor; not all the models used here include these two effects.

## 3.2 Annual mean climatology

The spread in the modeled annual & zonal mean distribution of water vapor is large and virtually all models are characterized by errors in their distribution of water vapor in the entire stratosphere. A few distinctions emerged between the two classes (HT and LT) of models. While the HT models capture the average representation of the large-scale circulation, there is a clear lack of its mean signal in the LT models. In some models (mainly LT models) there is also a clear lack of any representation of methane oxidation in the upper stratosphere (Figure 3.3). The main ingredients explaining biases in the representation of the stratospheric water vapor at the global level include the representation of convection, the cold point tropopause, cirrus clouds, convective mixing, large-scale transport within the stratosphere itself, and the representation of methane oxidation.

Figure 3.1 shows the bias (%) of the climatological water vapor for a subset of CMIP5 models (18 models, including COMBINE models) at 100 hPa in 4 regions as yearly means. In the tropics (20°S-20°N) models tend to show a negative bias, although with a large spread. There is no clear distinction of the bias between high horizontal/vertical resolution and low horizontal/vertical resolution models (not shown). At 20°-60°N/S latitudes, biases are instead mostly positive, leading therefore to generally smaller biases for the quasi-global average (compensation of errors). At 70 hPa (Figure 3.2), biases in general become larger especially at the global scale, given that the biases change sign at 20°-60°N/S latitudes in most models.

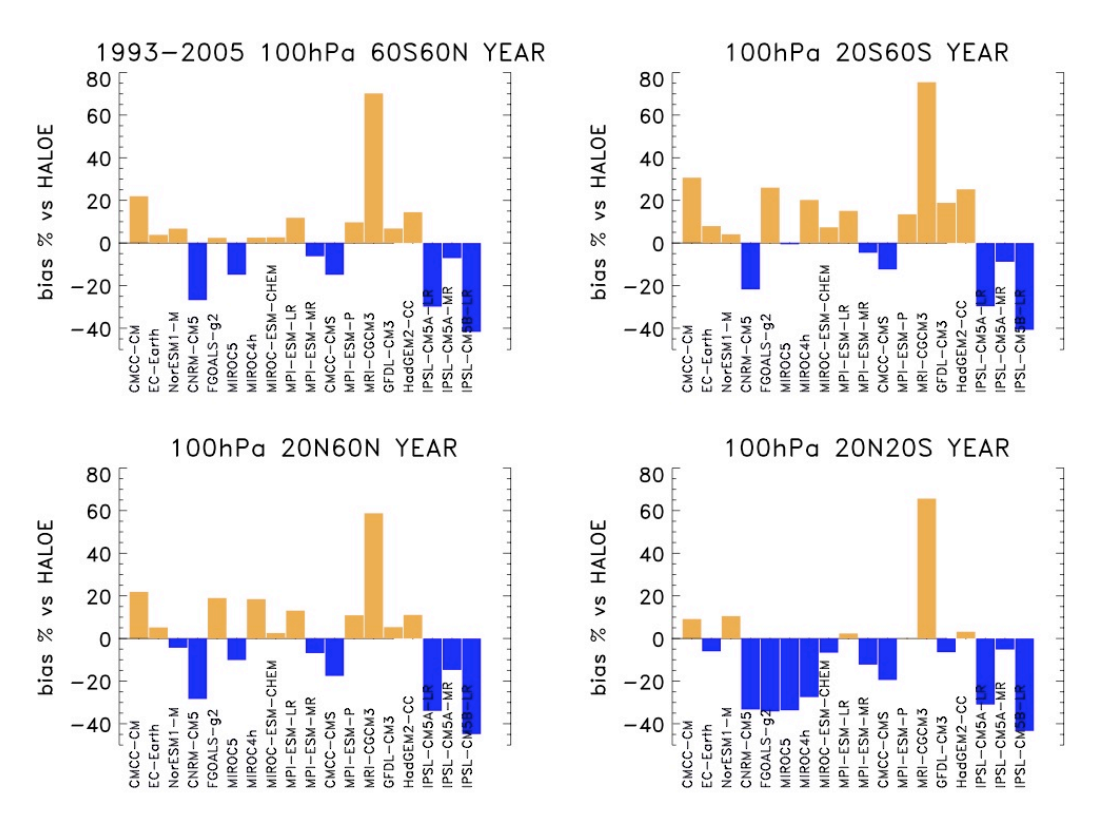


Figure 3.1: Biases (%) in modeled water vapor annual climatology at 100 hPa with respect to HALOE for the 1993-2005 period, at different latitude bands. Orange (blue) bars indicate positive (negative) biases.

If water vapor entering the lower stratosphere is expected to be mostly controlled by the temperature of the tropopause we could expect to find a relationship between the bias in the lower stratospheric water vapor at 20N-20S and the bias in the cold point temperature. Indeed, in our analysis we find a linear relationship between the bias in the 100hPa temperature (used as a proxy for the tropopause temperature) with respect to the ERA-Interim temperatures and the bias in water vapor with respect to HALOE across the models at 70 hPa in the DJFMAM season (not shown).

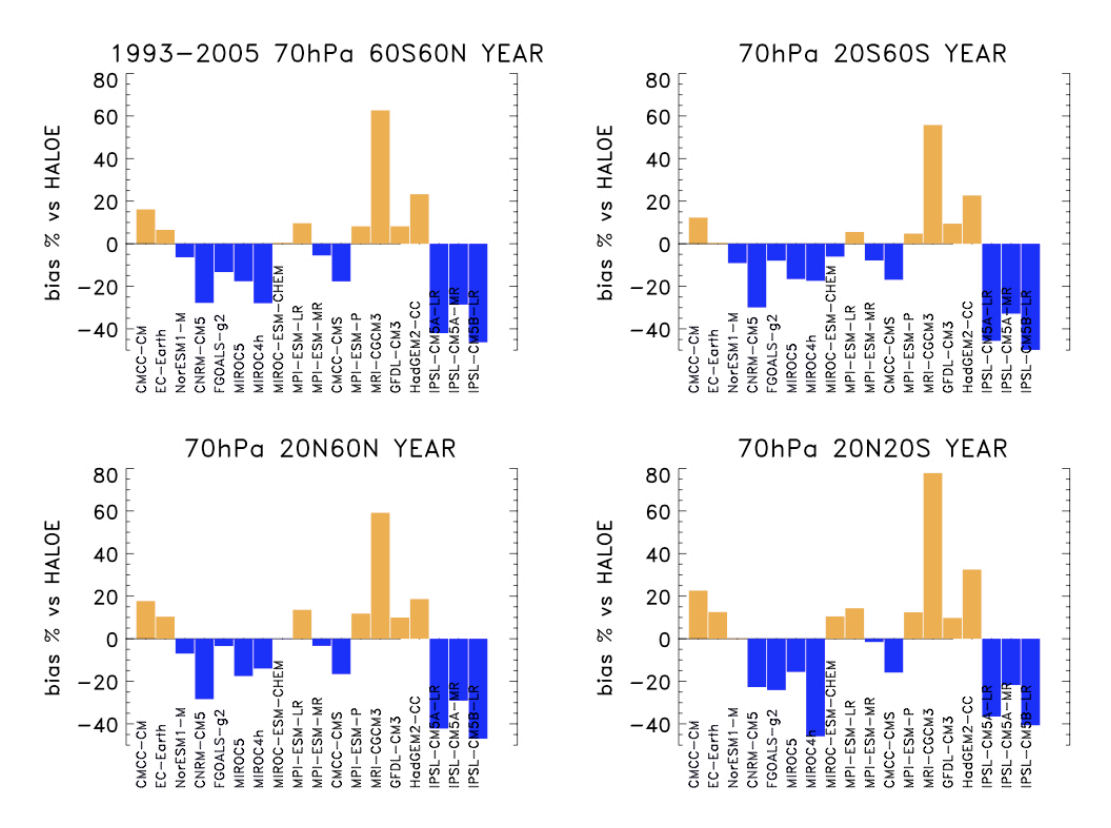


Figure 3.2: as Fig 1 but at 70 hPa

#### 3.3 Seasonal cycle

At seasonal time scales, the most striking feature in stratospheric water vapor is the tape recorder (Mote et al. 1996). Water vapor is a tracer in the lower stratosphere whose fluctuations are traced back to the Brewer Dobson Circulation changes at the tropopause. Any signal originating from the tropical lowermost stratosphere (including trends) tends to dissipate with increasing altitude in the tropics. Figure 3.3 shows the 10S-10N average water vapor climatology over 25 years for four HT multimodel average and for four LT multimodel average. Both HT and LT models show a seasonal cycle in water vapor, but the vertical propagation in time (e.g., the "tape recorder" effect") is better captured in the HT models.

### 3.4 Inter-annual variations: ENSO

Changes in the tropopause temperatures, tropical upwelling and deep convective activities have a large impact on stratospheric water vapor at inter-annual timescales. Inter-annual variations in stratospheric water vapor have mainly two causes: The inter-annual variability of stratospheric dynamics and the inter-annual variations in

the entry value of the water vapor mixing ratio, though these two processes are not independent (Dhomse et al. 2008). In the tropical stratosphere, the QBO is the dominant mode of inter-annual dynamical variability. Concerning the QBO, its signal in the water vapor anomalies is due to both QBO temperature-driven variations in the dehydration of air rising through the tropical tropopause and the QBO modulation of the ascent rate of tropical air and its redistribution due to QBO-induced mean meridional circulations (Giorgetta and Bengtsson 1999; Geller et al. 2002). The analysis of the subset of the COMBINE models that simulate the QBO reveals a clear QBO signature in the stratospheric water vapor anomalies (not shown). This signal has been shown to be dependent on the phase of ENSO (i.e. if the two signals are in phase or out of phase; Liang et al. 2011)

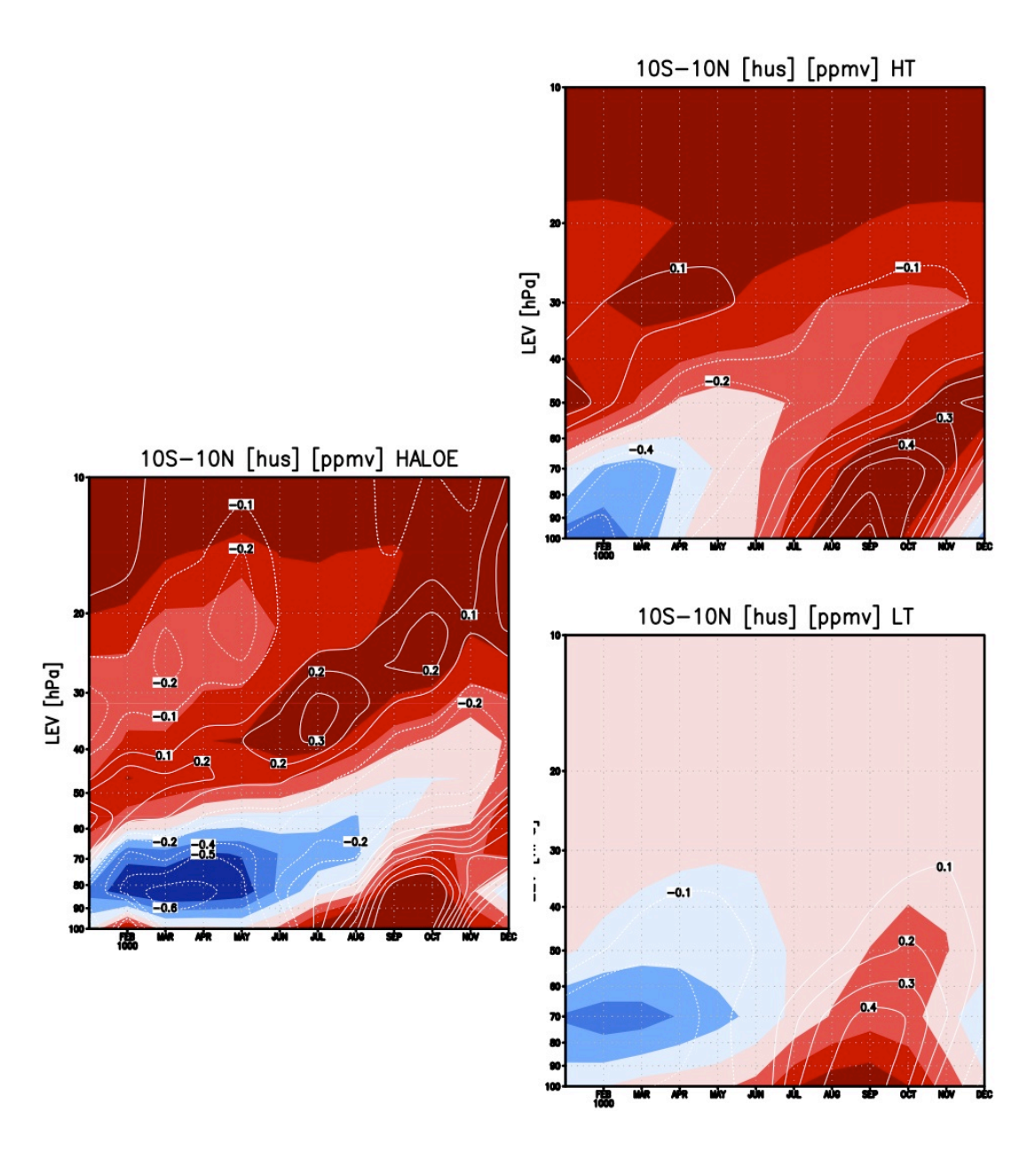


Figure 3.3: (left) 10°N-10°S monthly zonal mean water vapor (seasonal cycle) from HALOE. (right) 10°N-10°S HT (top) and LT (bottom) multi model mean of monthly zonal mean water vapor (seasonal cycle) over 25 years. Colors: from 2.4 to 3.8 ppmv every 0.2 ppmv; anomalies w.r.t the mean annual value are represented as white contours; white contour interval is 0.2 ppmv.

ENSO can modulate the stratospheric water vapor due to its impact on temperature and transport within the TTL (Gettelman et al. 2001). Strong El Nino events have been found to have an effect of moistening the lower stratosphere, whilst La Nina could lead to a reverse change of LS water vapor. El Nino events could change the location of water vapor minimum in the UT through modifying the large-scale circulation and convection in the Pacific. Moreover, SST changes associated to ENSO can modify the Brewer-Dobson circulation in the tropical LS. In this analysis we use the monthly mean temperature at 100 hPa as a proxy for the cold point temperature; in order to evaluate ENSO anomalies in models, we build composites based on the following definition:

An El Nino event is defined when the SST anomaly in the Nino3.4 region (5N-5S, 170W-120W) is larger than 1STD (calculated over the 1950-2005 period). Conversely, La Nina events have SST anomalies smaller than -1STD. El Nino and La Nina anomalies at 100hPa are calculated by compositing together the de-seasonalised time series.

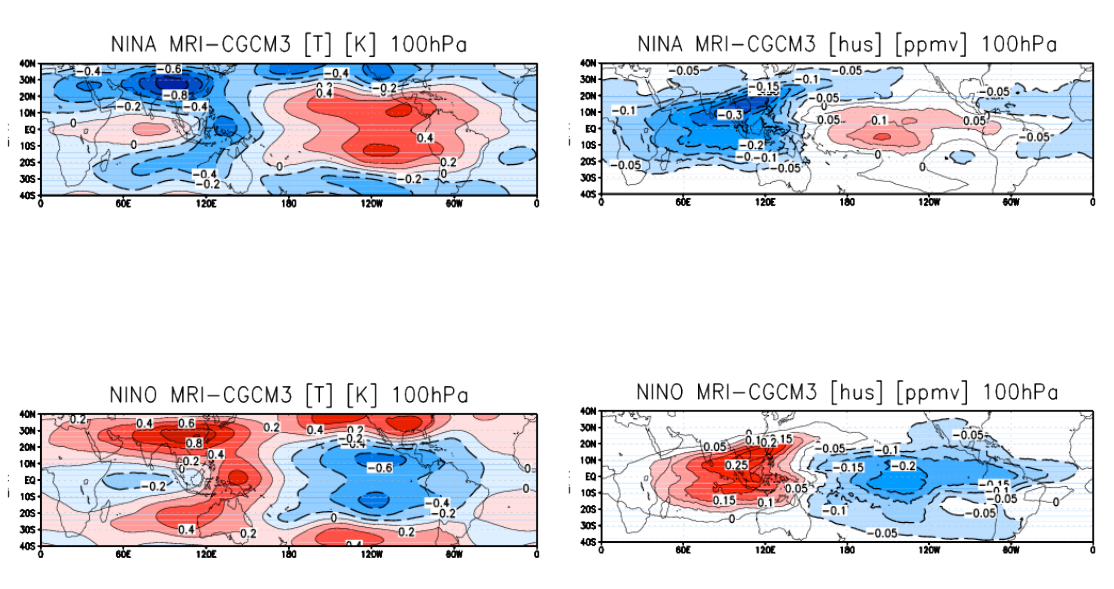
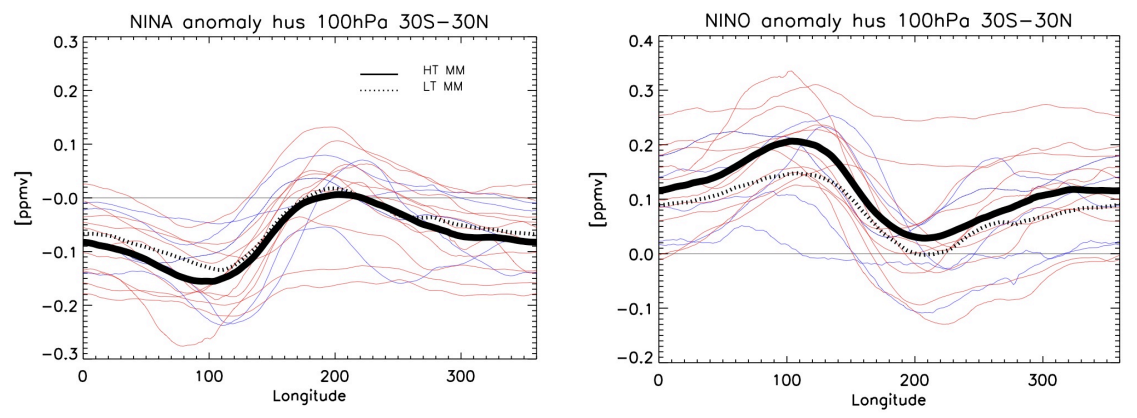


Figure 3.4: As an example of the composites (anomaly with respect to climatology): MRI-CGM3 El Nino and La Nina for temperature and water vapor, considering all ENSO events between 1850-2005. Contours for temperature are shown every 0.2K, from -0.8K to 0.8K; contours for water vapor are shown from -0.4 ppmv to 0.4ppmv, every 0.05ppm, therefore red (blue) contours are shown for anomalies larger (smaller) than 0.05 (-0.05).

In Figure 3.4 the composites in temperature and water vapor at 100 hPa are shown for one specific model as an example. The pattern of temperatures shows a high degree of zonal asymmetry with an increase of temperature of about 0.4 K in the west Pacific (near 135E) and a decrease of about -0.6 K between 180 and 270E. ENSO produces an anti-correlation between SSTs and temperatures: warmer SSTs are associated to larger convection and therefore lower temperatures aloft. The signal is also larger off the equator near 20 degrees lat. This pattern and its magnitude are in good agreement with observations when similar composites are analyzed (thought for a different period). The majority of the models are able to reproduce the observed El Nino signal in the tropopause temperature and show a pattern that is very similar to the one shown here (independently if they are HT or LT models). The water vapor distributions of El

Nino variability are instead much more spread across the models even if they are always reporting a clear moistening effect of the El Nino phase, that appears more evident when looking at Figure 3.5, described below. The patterns for La Nina are almost symmetric in longitude for temperature and water vapor with again a large spread in the water vapor patterns of variability, however with a clear drying global effect. Larger spread is expected because variations in the tropopause temperature are non-linearly correlated with the water vapor anomalies and strongly depend on the background mean state. At 70 hPa (not shown) the moistening (drying) effect of El Nino (La Nina) are confirmed in all models. We have also analysed the low frequency ENSO tape recorder (not shown) that impacts the water vapor by modulating the cold point temperature. The HT and LT models both show a positive (negative) anomaly of water vapor that propagates upward from the tropical regions during El Nino (La Nina), with a quicker and less pronounced signal in the LT (not shown). This result again confirms that if the representation of the tropopause temperature is due to a large number of factors in models, once the water vapor anomaly reaches the lower stratosphere its transport is more realistically represented in the HT than in the LT models, because of the better representation of the large-scale transport within the stratosphere itself.



*Figure 3.5:* Composite of Figure 3.4 averaged between 30S-30N, HT models in red, LT models in blue. Thick continuous black line is the HT multi-model average, dotted line is the multi-model LT average.

Figure 3.5 summarizes the ENSO impact on atmospheric water vapor at 100 hPa and 30°S-30°N. The signal shows a large spread across the models, with a clear moistening effect of El Nino west of the date line. There is a better agreement among models for the La Nina drying effect over the west Pacific and over Indonesia than for the El Nino moistening effect over the warm pool region. There is not a clear distinction between HT and LT models. This is possibly due to the fact that the factors controlling the representation of the tropopause temperature in models are numerous, with the UT resolution being just one of these. By looking at the HT and LT multi model averages (continuous and dotted lines, respectively) it appears that there is a larger signal in the HT models during El Nino. The difference between HT and LT is however much smaller than one standard deviation of the responses across the models.

The global impact of ENSO variations on the global water vapor can be much different across the models. Indeed the models do represent very large biases in the

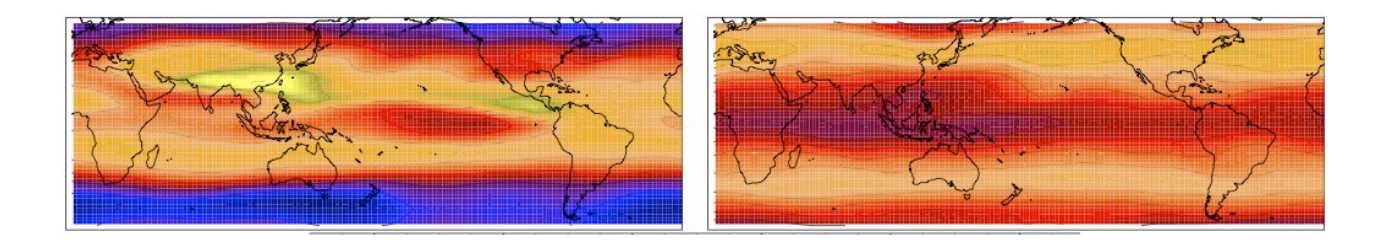
amplitude and frequency of ENSO events, with their spectra reporting large discrepancies in the historical period with respect to HadISSTs observations (not shown, please also refer to Bellenger et al. in press). This implies that even if the average ENSO response in stratospheric water vapor can be considered correct (thought as seen there is a large spread across the models), if the representation of ENSO itself, in terms of amplitude and frequency of occurrence, is largely biased the global effect of ENSO on water vapor can lead to biases in long-term averages and trends. The misrepresentation of ENSO in models is associated to several aspects: the representation of the mean state, the atmospheric resolution, the parameterization of convection, the atmosphere-ocean coupling strength, the parameterization of the boundary layer, the representation of the oceanic component (Guilyardi et al. 2005).

#### 3.5 Inter-annual variations: Asian Monsoon

The Asian Monsoon anticyclone has been recently identified as a key transport region of air masses from the troposphere deep into the stratosphere (e.g. Randel et al. 2010). We have therefore analysed the interannual variations of lower stratospheric water vapor in models associated to the Asain Monsoon anticyclone. Figure 3.6 shows the linear correlation between the time series of the monsoon anticyclone monthly mean area at 100 hPa, defined as detailed in the paragraph below, and the water vapor at 80hPa for the piControl simulation of one specific model (the CMCC-CMS) at four different seasons; the correlation is shown for each grid point (i.e. each water vapor anomaly time series has been correlated to the Asian Monsoon anticyclone index). The Asian Monsoon anticyclone index has been constructed as follows: from the monthly mean July and August time series of the geopotential height (Z) at 100 hPa, a probability distribution (PDF) function of Z, averaged between 20°E and 120°E, versus latitude (in the range 0°-60°N) has been built. From this PDF, the 90%th percentile of the PDF has been estimated and defined as a reference value for the monsoon area for each model. Before estimating the PDF, Z has been interpolated on a 1 deg grid, in order to avoid differences across the models derived from a different spatial resolution. Then, for each month of the 500 years time series, the index is built by measuring the area (in Km<sup>2</sup>) enclosed by this contour. In order to avoid including contours in wrong areas, the contour is searched in regions eastward of 20W and northward of the Equator. The July and August indices have then been averaged together in order to have a time series of one value per year, representing variations of the summertime Asian monsoon anticyclone area. Correlations between this index and the water vapor shown in Figure 3.6 (top-left) reveal that in this model, there is a high correlation between the global water vapor at 80hPa in JJA and the area of the anticyclone in the same year (year0). This correlation is especially strong in the NH over the Asian Monsoon Anticyclone region, indicating the role of this region as a summer entry point for the stratospheric water vapor. The correlation then reduces in the following season (SON of year0, Figure 3.6 top-right), however maintaining a positive correlation at non-equatorial latitude bands, indicating that variations of water vapor in this season maintains a memory of their entry point value and that water vapor from the entry point is then transported by the large scale circulation. Correlations then strongly reduce in the following seasons (DJF of year+1 and MAM of year+1, Figure 3.6 bottom). The same index has been estimated for all the models for the piControl and the historical simulations. Composites of water vapor during high and low years of the anticyclone area in the lower stratosphere indicate that the anticyclone is modulating the vertical distribution of water vapor in the majority of the models (not shown). Moreover, clear large trends appear in the anticyclone indices in all the *historical* simulations of all models (not shown).

hus 80hPa JJA y0 AM JA 100hPa

hus 80hPa SON y0 AM JA 100hPa



hus 80hPa DJF y1 AM JA 100hPa

hus 80hPa MAM y1 AM JA 100hPa

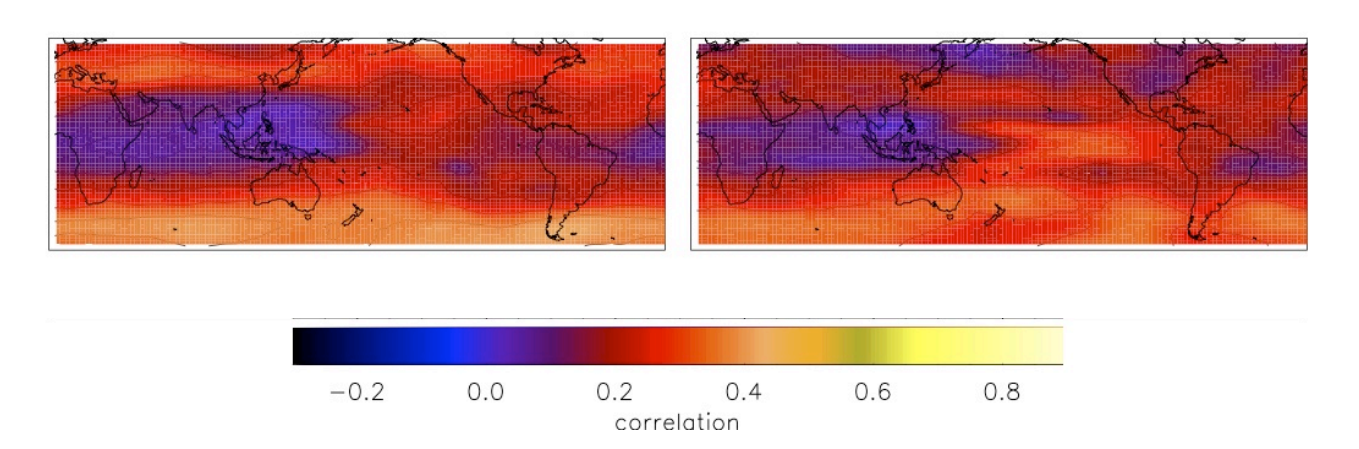


*Figure 3.6;* Linear correlations of the Asian Monsoon anticyclone index and the water vapor at 80hPa in the 500-yr piControl simulation of the CMCC-CMS model, at 4 seasons (see text for details)

#### 6. Trends

All the model simulations reproduce a clear positive trend in the global lower stratospheric water vapor in the 1980-2005 period in different seasons (Figure 3.7) that is found to be consistent with a positive trend in the 100hPa temperature (not shown). In our analysis we have found that all models reproduce a positive trend in the warm ENSO phase frequency of occurrence: i.e. the number of months with a warm ENSO anomaly larger than 1 standard deviation within a decade is increasing from the 80's to the 90's and to 2000's, whereas in observation this increasing frequency is not found. However, the most sensitive models with respect to the water vapor variations associated to warm ENSO are also the models showing the largest trend in the LS water vapor in DJFMAM (not shown). The fact that this relationship is not valid for the JJASON trend in water vapor, confirms the role of warm ENSO related tropopause temperature variations because the DJFMAM water vapor in the lower stratosphere (differently from JJASON lower stratospheric water vapor) is mainly controlled by the tropopause temperature (Randel and Jensen 2013) and

therefore if models do show an increase in the warm ENSO occurrence, this could explain the positive trends in DJFMAM water vapor. This could also possibly explain why no model is able to reproduce any clear decadal signal of water vapor that was found in observations from 1990 to today, at least for the DJFMAM season.

Concerning the JJA season, as the models are sensitive to variations in the Asian Monsoon anticyclone area and this area is shown to linearly increase in the 1950-2005 period (not shown), it is possible that these trends are playing a role in the water vapor increase reported by models during this season.

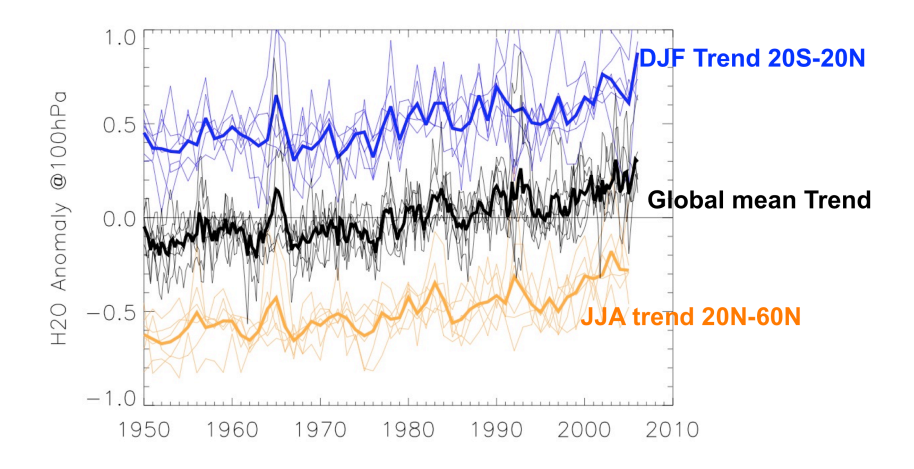


Figure 3.7: Time series of nearly global (60S-60N) annual mean water vapor at 100 hPa for a subset of CMIP5 models (black lines) and their multi-model average (black thick line) together with the time series of the 20S-20N DJF and 20N-60N JJA water vapor.

### References

- Bellenger H., et al. (2013) ENSO representation in climate models: from CMIP3 to CMIP5. Clim. Dyn., in press.
- Dhomse, S., M. Weber, J. Burrows (2008) The relationship between tropospheric wave forcing and tropical lower stratospheric water vapor. Atmos. Chem. Phys., 8, 471-480, doi:10.5194/acp-8-471-2008.
- Fueglistaler, S., P. H. Haynes (2005) Control of interannual longer-term variability of stratospheric water vapor. J. Geophys. Res., 110, D24108, doi:10.1029/2005JD006019.
- Geller, M. A., X. Zhou, M. Zhang (2002) Simulations of the Interannual Variability of Stratospheric Water Vapor. J. Atmos. Sci., 59, 1076–1085.
- Gettelman, A., W. J. Randel, S. Massie, F. Wu, W. G. Read, J. M. Russell III (2001) El-Nino as a natural experiment for studying the tropical tropopause region. J. Climate, 14:3375-3392.
- Giorgetta, M.A., L. Bengtsson (1999) Potential role of the quasi-biennial oscillation in the stratosphere-troposphere exchange as found in water vapor in geral circulation model experiments. J. Geophys. Res., 104, 6003-6019.
- Guilyardi E., et al. (2004) Representing El Niño in coupled ocean-atmosphere GCMs: the dominant role of the atmospheric component. J. Climate, 17:4623-4629
- Liang, C. K., et al. (2011) Record of tropical interannual variability of temperature and water vapor from a combined AIRS-MLS data set. J. Geophys. Res., 116, D06103, doi:10.1029/2010JD014841.
- Mote, P. W., et al. (1996) An atmospheric tape recorder: The imprinting of tropical tropopause temperatures on stratospheric water vapor. J. Geophys. Res. 101, 3989–4006
- Randel, W.J., et al. (2010) Asian monsoon transport of pollution to the stratosphere. Science, 328, 611, doi:10.1126/science.1182274
- Randel, W. J., E. J. Jensen (2013) Physical processes in the tropical tropopause layer and their roles in a changing climate. Nature Geoscience, 6, 169–176. doi: 10.1038/ngeo1733,
- Solomon, S., et al. (2010) Contributions of Stratospheric Water Vapor to Decadal Changes in the Rate of Global Warming. Science: 327 (5970), 1219-1223.